BIOCHEMISTRY
including biophysical chemistry & molecular biology
Article

Biochemistry **2010,** *49,* 10013–10023 10013
DOI: 10.1021/bi100855a

Electron Transfer of Site-Specifically Cross-Linked Complexes between Ferredoxin and Ferredoxin−NADP$^+$ Reductase[†]

Yoko Kimata-Ariga,*[,‡] Yukiko Sakakibara,[‡] Takahisa Ikegami,[§] and Toshiharu Hase[‡]

[‡]*Laboratory of Regulation of Biological Reactions and* [§]*Laboratory of Structural Proteomics, Institute for Protein Research, Osaka University, 3-2 Yamadaoka, Suita, Osaka 565-0871, Japan*

Received May 27, 2010; Revised Manuscript Received September 14, 2010

ABSTRACT: Ferredoxin (Fd) and Fd-NADP$^+$ reductase (FNR) are redox partners responsible for the conversion between NADP$^+$ and NADPH in the plastids of photosynthetic organisms. Introduction of specific disulfide bonds between Fd and FNR by engineering cysteines into the two proteins resulted in 13 different Fd−FNR cross-linked complexes displaying a broad range of activity to catalyze the NADPH-dependent cytochrome *c* reduction. This variability in activity was thought to be mainly due to different levels of intramolecular electron transfer activity between the FNR and Fd domains. Stopped-flow analysis revealed such differences in the rate of electron transfer from the FNR to Fd domains in some of the cross-linked complexes. A group of the cross-linked complexes with high cytochrome *c* reduction activity comparable to dissociable wild-type Fd/FNR was shown to assume a similar Fd−FNR interaction mode as in the native Fd:FNR complex by analyses of NMR chemical shift perturbation and absorption spectroscopy. However, the intermolecular electron transfer of these cross-linked complexes with two Fd-binding proteins, nitrite reductase and photosystem I, was largely inhibited, most probably due to steric hindrance by the FNR moiety linked near the redox center of the Fd domain. In contrast, another group of the cross-linked complexes with low cytochrome *c* reduction activity tends to mediate higher intermolecular electron transfer activity. Therefore, reciprocal relationship of intramolecular and intermolecular electron transfer abilities was conferred by the linkage of Fd and FNR, which may explain the physiological significance of the separate forms of Fd and FNR in chloroplasts.

In plants, ferredoxin (Fd)[1] and Fd-NADP$^+$ reductase (FNR) are redox partners, responsible for the reduction of NADP$^+$ at the end of the photosynthetic electron transfer chain. Both proteins also catalyze the reverse reaction, i.e., the oxidation of NADPH to supply the reducing power for heterotrophic metabolism under nonphotosynthetic conditions (*1*). FNR is a prototype for a family of flavin-containing electron transferases displaying common structural properties called the "FNR-like module": a two-domain module with one domain binding the flavin and the other binding pyridine nucleotide (*2*, *3*). The function shared by the proteins in the FNR family is the flavin-dependent conversion between two-electron reactions with pyridine nucleotides and one-electron reactions with carriers. The one-electron carriers are, in some cases, independent proteins such as plant-type Fd, but in other cases they are found in domains fused to the N- or C-terminus of the two-domain modules. For example, phthalate dioxygenase reductase (PDR) carries a Fd-like domain attached to its C-terminus (*2*), and benzoate dioxygenase reductase (BenC) has a similar domain at its N-terminus (*4*).

The X-ray crystal structures of the plant-type Fd:FNR complexes (*1*, *5*, *6*) clarified the sites involved in complex formation between the Fd and FNR molecules. The redox centers in the complexes, the [2Fe-2S] cluster of Fd and flavin adenine dinucleotide (FAD) of FNR, are located in close proximity (i.e., 6−8 Å). The basic pattern consists of a core of hydrophobic interactions surrounding the prosthetic groups, stabilized by a series of interactions between charged side chains and through hydrogen bonds. However, the specific interaction mode of Fd and FNR, such as the orientation of Fd relative to FNR, is largely different among the three known X-ray structures of Fd/FNR pairs from maize leaf and root tissues and the cyanobacterium *Anabaena*, which exhibit distinct physicochemical and physiological properties (*1*). Furthermore, alignment of the X-ray structures of PDR and BenC, the monomeric iron−sulfur flavoprotein reductases mentioned above, together with any of the three Fd:FNR complexes, showed significant differences in the location of the Fd domain relative to the corresponding flavin-containing domain among all combinations (*4*). Therefore, configuration of Fd and FNR modules can be variable as long as adequate distance between the iron−sulfur cluster and flavin cofactor is maintained. Such variability is expected to correlate with the differences in their physiological functions such as the nature of specific downstream partner proteins as well as the direction and efficiency of electron transfer.

[†]This work was supported by grant in aids for Creative Scientific Research (15GSO320) and for Scientific Research on Priority Areas (13225001) from the Ministry of Education, Culture, Sports, Science, and Technology of Japan.

*To whom correspondence should be addressed. Tel: +81-6-6879-8611. Fax: +81-6-6879-8613. E-mail: a-yoko@protein.osaka-u.ac.jp.

[1]Abbreviations: Fd, ferredoxin; FNR, ferredoxin-NADP$^+$ reductase; FAD, flavin adenine dinucleotide; cyt *c*, cytochrome *c*; PDR, phthalate dioxygenase reductase; BenC, benzoate dioxygenase reductase; NiR, nitrite reductase; FNR_{sq}, FNR in the semiquinone state; FNR_{red}, FNR in the reduced state; FNR_{ox}, FNR in the oxidized state; Fd_{ox}, Fd in the oxidized state; Fd_{red}, Fd in the reduced state; HSQC, heteronuclear single-quantum correlation; PS I, photosystem I.

Published on Web 10/18/2010

There have been many trials to artificially connect the naturally separated redox modules by cross-linking (*7*−*10*) and genetically fusing (*11*−*13*) or, conversely, to separate the naturally linked domains by enzymatic digestion (*14*) and genetic manipulation (*15*) for the purpose to dissect the mechanism of electron transfer or to stabilize the complex of dissociable partner proteins. In the case of the reductase component of soluble methane monooxygenase from *Methylococcus capsulatus* (MMOR), which shares a common domain organization with BenC, separation of the Fd domain from the FNR-like module resulted in extremely slow electron transfer between the two domains, indicating that cofactor proximity is essential for efficient electron transfer (*15*). Also, natural flavocytochrome $P450_{BM3}$, in which cytochrome P450 protein and P450 reductase enzyme (FAD- and FMN-containing NADPH-binding protein) are covalently fused, exhibits much higher reaction velocity compared to conventional P450 systems composed of separate P450 protein and its partner reductase, although electron transfer was shown to occur between monomers of the dimeric form of $P450_{BM3}$ (*16*). For plant Fd/FNR, there have been two reports on cross-linking resulting in different electron transfer properties probably due to the different cross-linking conditions (*9*, *10*) and one report for a genetic fusion (*11*). One of the cross-linked complexes and the genetic fusion were functionally active in terms of electron transfer from the FNR to the Fd moiety and reduction of redox proteins such as cytochrome *c* (cyt *c*), while the other cross-linked complex was inactive.

Understanding the mechanisms of electron transfer between redox proteins is a complex problem involving specific recognition between redox partners, subsequent conformational changes, and electron transfer between redox centers which is proposed to be mediated through a polypeptide path or by direct transfer. Formation of a transient complex allows the two redox centers to assume appropriate orientations required for the rapid electron transfer. The rate of electron transfer depends on the difference in redox potential, distance, and relative orientation between the two redox centers, as well as on the energy required for nuclear rearrangement upon charge transfer, according to the Marcus theory (*17*). Our goal is to clarify the relative contribution of these factors to the electron transfer between the two redox partners, Fd and FNR. In this study, we have prepared a series of cross-linked complexes of maize leaf Fd and FNR by introducing, in each case, a specific disulfide bond between the two proteins, so that the two protein moieties assume various configurations. These Fd−FNR cross-linked complexes showed diverse structural and electron transfer properties. Preliminary results have been presented at the Sixteenth International Symposium on Flavins and Flavoproteins (*18*).

EXPERIMENTAL PROCEDURES

Production and Purification of Fd−FNR Cross-Linked Complexes. Five Fd mutants (A1C, D21C, S53C, S59C, and A70C) and three FNR mutants (E19C, E25C, and E36C), each containing one substituted cysteine residue at the surface of *Zea mays* leaf-type Fd (Fd I) (*19*) and FNR (L-FNR I) (*20*), respectively, were prepared using a QuikChange mutagenesis kit (Stratagene). The mutant Fd and FNR proteins were expressed and purified from *Escherichia coli* BL21 (DE3) Gold cells harboring the above constructs, according to the methods described previously (*19*, *20*). All mutant proteins were purified as homodimers but separated into monomers by addition of β-mercaptoethanol (5% v/v) just before cross-linking. Thirteen kinds of Fd−FNR cross-linked complexes were produced by incubation of various combinations of each one of the Fd and FNR mutants at about 3 mM in 50 mM Tris-HCl, pH 7.5, and 100 mM NaCl at 4 °C for 2−3 days. Formation of the cross-linked complexes was monitored with gel-filtration chromatography (Sephadex G-75) in 50 mM Tris-HCl, pH 7.5, and 150 mM NaCl, and the resulting complexes were purified by ion-exchange chromatography (DEAE-cellulose) with a linear gradient of 0−0.5 M NaCl in 50 mM Tris-HCl, pH 7.5. Quantification of the Fd−FNR cross-linked complexes was performed according to the method described for a chimeric Fd/FNR fusion protein (*11*).

Enzymatic Analysis. Unless otherwise specified, NADPH-dependent cyt *c* reductase activity of Fd−FNR cross-linked complexes and dissociable wild-type Fd/FNR was measured as described previously (*20*) by monitoring the increase of reduced cyt *c* at 550 nm (in a cuvette with 2 mm light path) in the reaction mixture containing 100 μM NADPH, 250 μM cyt *c*, 20 nM Fd−FNR cross-linked complex, 50 mM Tris-HCl, pH 7.5, and 100 mM NaCl in the presence of the NADPH-generating system at room temperature. A control experiment was performed with dissociable wild-type Fd/FNR by adding 20 nM FNR and 40 μM (saturating amount) Fd instead of the cross-linked complex; the K_m value of FNR for Fd in the cyt *c* reduction has been reported to be 3−10 μM (*19*, *20*). This yielded a catalytic activity of 120 ± 12 mol of cyt *c* reduced (mol of FNR)$^{-1}$ s^{-1}. NADPH-dependent nitrite reductase (NiR) activity via FNR and Fd was measured as described previously (*21*) as the rate of consumption of nitrite in the reaction mixture containing 200 μM NADPH, 200 μM $NaNO_2$, 20 nM recombinant NiR from *Synechocystis* sp. PCC 6803 (*21*), 2 μM Fd−FNR cross-linked complex, 50 mM Tris-HCl, pH 7.5, and 100 mM NaCl in the presence of the NADPH-generating system at room temperature. A control experiment was performed by adding 100 nM FNR and 2 μM Fd instead of the cross-linked complex. This resulted in a catalytic activity of 1.21 ± 0.13 mol of nitrite reduced (mol of NiR)$^{-1}$ s^{-1}. Consumption of nitrite was measured by colorimetric reaction with *N*-(1-naphthyl)ethylenediamine after diazotization with sulfanilamide, according to the method described previously (*22*). Photoreduction of $NADP^+$ via Fd and FNR was measured as described previously (*23*) by monitoring the increase of NADPH at 340 nm during illumination in the reaction mixture containing 200 μM $NADP^+$, 1 μM Fd−FNR cross-linked complex, 10 μg of chlorophyll/mL of spinach (*Spinacia oleracea*) thylakoid membranes, 50 mM HEPES−NaOH, pH 7.5, 100 mM NaCl, and 1 mM $MgCl_2$ at room temperature. A control experiment was performed by adding 1 μM Fd instead of the cross-linked complex, resulting in a catalytic activity of 14.3 ± 0.5 nmol of NADPH formed (μg of chlorophyll)$^{-1}$ s^{-1}.

Stopped-Flow Analysis. The electron transfer processes between NADPH and the Fd−FNR cross-linked complexes were studied using an Applied Photophysics SX. 18MV spectrophotometer at 25 °C. All samples were made anaerobic before introduction into the stopped-flow syringes by successive evacuation and flushing with O_2-free Ar. All of the reactions were carried out in 50 mM Tris-HCl, pH 7.5, and 100 mM NaCl. Final concentrations of 10 μM were used for NADPH and Fd−FNR complexes, and 10 μM FNR and 10−40 μM Fd were used for separate wild-type Fd/FNR, unless otherwise specified. Changes in absorbance were used to follow the reaction, either in single-wavelength mode or in a spectral range between 240 and 700 nm

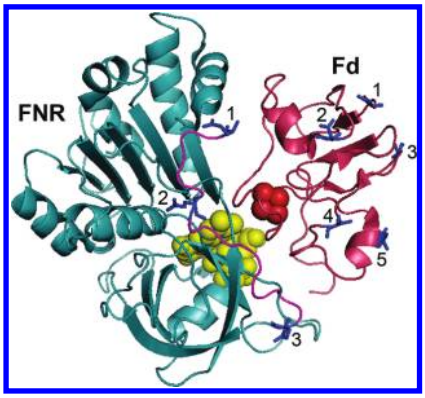

FIGURE 1: Ribbon diagram of the crystal structure of maize leaf Fd:FNR complex (*5*). The prosthetic groups, FAD, and the [2Fe-2S] cluster are drawn as spheres. The locations of the residues that were substituted to cysteine residues in each molecule are shown with a stick model. For FNR, 1, 2, and 3 correspond to Glu19, Glu25, and Glu36, respectively, and for Fd, 1−5 correspond to Ala1, Asp21, Ser53, Ser59, and Ala70. The N-terminal loop region up to position 36 of FNR is shown in magenta. The first N-terminal 18 residues are not visible in this crystal structure.

using a photodiode array detector. Single wavelength absorption data and multiple wavelength absorption data were collected and processed using the SX. 18MV software and X-SCAN software of Applied Photophysics, respectively.

Spectroscopic Analysis. The NMR chemical shift perturbation experiment was performed basically according to the procedure described previously (*24*, *25*). Recombinant maize leaf Fds (wild-type, D21C, and S59C) were labeled uniformly with ^{15}N-stable isotope. NMR spectra were recorded at 298 K on a Bruker AV-400 M spectrometer, operated at 400.13 MHz for the proton base frequency. For measurements of Fd−FNR cross-linked complexes, ^{15}N-labeled D21C and S59C Fd mutants and non-labeled FNR cys mutants (E19C and E36C) were reacted in different combinations, and the resulting ^{15}N-labeled Fd−FNR cross-linked complexes were purified as described above. All of the NMR samples, except those used for the titration experiment of wild-type Fd/FNR, were measured at 0.2 mM protein concentration in a 30 mM potassium phosphate buffer (pH 7.0) containing 100 mM KCl and 10% D_2O in the presence or absence of DTT (at 4 mM). Weighted averages of the ^{1}H and ^{15}N chemical shift changes were calculated with the equation $\Delta\delta = [(\Delta\delta_{^1HN})^2 + (0.17\Delta\delta_{^{15}N})^2]^{1/2}$. All of the spectra were processed with NMRPipe software (*26*) and analyzed with Sparky software developed by T. D. Goddard and D. G. Kneller in UCSF.

Absorption spectra of wild-type or mutant Fd/FNR and Fd−FNR cross-linked complexes were measured at 25 °C using a spectrophotometer (model UV-2500; Shimadzu) under different conditions.

RESULTS

Preparation of Fd−FNR Cross-Linked Complexes. As linkage sites between Fd and FNR, we have chosen residues with location on the respective protein surface, whose side chains protrude externally without being involved in the binding area of the native Fd:FNR complex; this should avoid direct interference with the binding between Fd and FNR (Figure 1). Three FNR residues, surrounding the FAD binding site, were chosen because any linkage using FNR residues located far from FAD was expected to cause poor electron transport to Fd. On the Fd side, five residues at various distances from the [2Fe-2S] cluster were

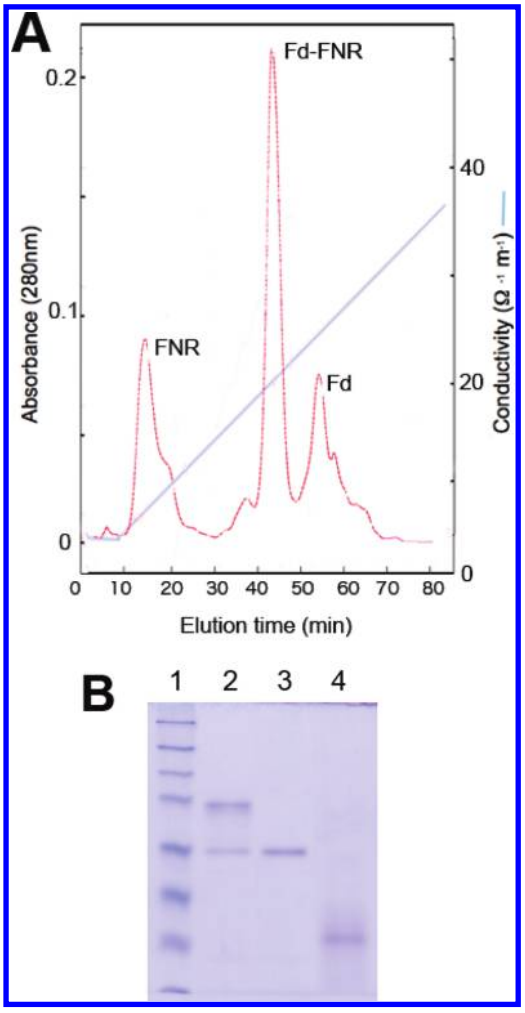

FIGURE 2: Ion-exchange chromatography (A) and SDS−PAGE analysis under nonreducing condition (B) of the reaction for the Fd−FNR cross-linked complex formation. (A) The elution profile for the reaction between Fd5C and FNR1C mutants is shown as an example; the Fd−FNR cross-linked molecule eluted between the retention time of Fd and FNR from DEAE-Toyopearl FPLC column applying a linear gradient of 0−0.5 M NaCl (shown as conductivity). According to the absorption spectra, the other minor peaks are probably derived from multiple conformations of the Fd−FNR complex and Fd−Fd/FNR−FNR homodimers, respectively. The chromatographic profiles of all 13 reactions were basically the same. (B) An example of SDS−PAGE (12.5% polyacrylamide) analysis for the reaction between Fd2C and FNR2C is shown. Lane 1, molecular weight markers (mass values in kDa are as follows: 175, 83, 62, 47.5, 32.5, 25, 16.5, 6.5); lane 2, reaction mixture of Fd2C and FNR2C; lane 3, FNR2C (the same molar equivalent of lane 2); lane 4, Fd2C (8-fold molar equivalent of lane 2). The band with apparent molecular mass of 46.5 kDa in lane 2 corresponds to the expected mass of the Fd−FNR cross-linked complex (10.5 kDa Fd plus 35.3 kDa FNR). Fd is generally less stained with Coomassie brilliant blue on SDS−PAGE, and therefore the Fd band in lane 2 is hard to be detected. Fd yields a higher mass value by SDS−PAGE, due to its high content of negative charges.

selected. Because Fd is a small molecule of ~11 kDa, it was expected that the surface-exposed [2Fe-2S] cluster may receive electrons from FNR even if it is linked in orientations largely different from that observed in the native Fd:FNR complex.

Each of these residues was substituted by a cysteine residue, resulting in five Fd and three FNR mutants named Fd1C−5C and FNR1C−3C, respectively, according to the mutation sites numbered in Figure 1. By incubating the different combinations of Fd and FNR Cys mutants together, Fd−FNR cross-linked

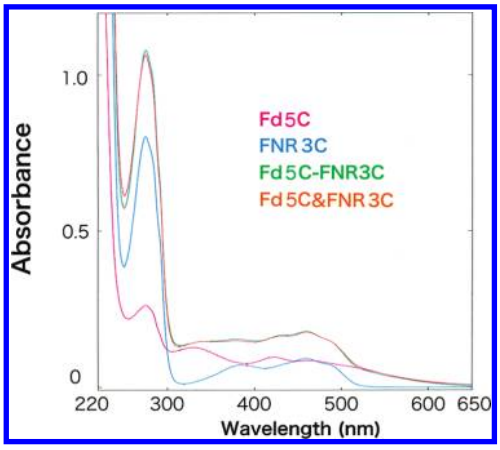

FIGURE 3: Absorption spectra of the purified Fd−FNR cross-linked complex and individual Fd and FNR mutants. An example of the spectra of Fd5C, FNR3C, and their cross-linked complex (Fd5C−FNR3C) at 10 μM in 50 mM Tris-HCl, pH 7.5, and 150 mM NaCl, together with the computed spectrum of an equal amount of the Fd and FNR (Fd5C and FNR3C) is shown.

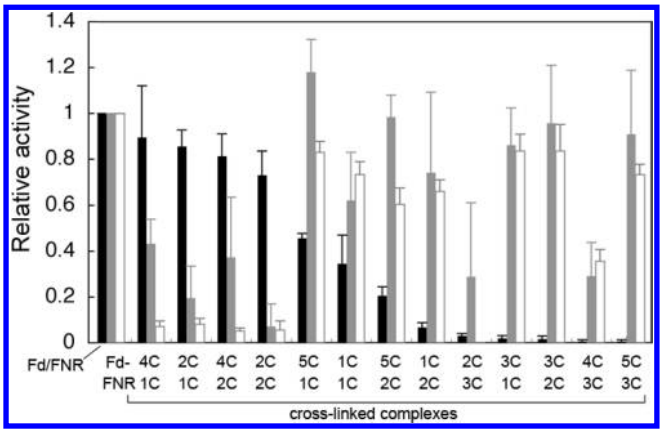

FIGURE 4: Activities of NADPH-dependent cyt *c* reduction (black bars), nitrite reduction (gray bars), and photoreduction of $NADP^+$ (white bars) with dissociable wild-type Fd/FNR and Fd−FNR cross-linked complexes in descending order of cyt *c* reduction activity, presented as the ratios relative to those of the wild-type Fd/FNR. Each measurement was performed under nonsaturating conditions for the complexes. Activities of wild-type Fd/FNR in these three assays are 120 ± 12 mol of cyt *c* reduced (mol of FNR)$^{-1}$ s^{-1}, 1.21 ± 0.13 mol of nitrite reduced (mol of NiR)$^{-1}$ s^{-1}, and 14.3 ± 0.5 nmol of NADPH formed (μg of chlorophyll)$^{-1}$ s^{-1}, respectively. Reaction conditions are described in Experimental Procedures.

complexes were preferentially formed over Fd−Fd and FNR−FNR homodimers with all 13 combinations we tried, although the rate of the reactions varied depending on the combination. This is probably because of the preferential electrostatic attraction between Fd that contains a high proportion of negatively charged residues and FNR that has a cluster of positively charged residues around its Fd-binding region. Formation of Fd−FNR cross-linked complexes was confirmed by ion-exchange chromatography (Figure 2A) and SDS−PAGE analysis (Figure 2B) with apparent molecular mass of 46.5 kDa. Absorption spectra of the purified complexes nearly match the computed spectrum of an equal amount of Fd and FNR (Figure 3), indicating the content of one [2Fe-2S] cluster and one FAD per complex.

NADPH-Dependent Cyt c Reductase Activity (NADPH/FNR/Fd/Cyt c). The electron transport from NADPH to Fd via FNR is routinely measured *in vitro* through a coupled assay, using cyt *c* as final electron acceptor. The constructed 13

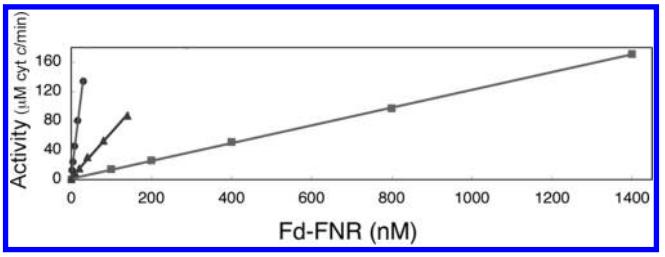

FIGURE 5: NADPH-dependent cyt *c* reductase activities at various concentrations of Fd2C−FNR1C (group I, closed circle), Fd1C−FNR1C (group II, closed triangle), and Fd5C−FNR3C (group III, closed square) cross-linked complexes. Reactions were performed in the presence of different concentrations of each complex. Examples of representative complexes from each group described in the text are shown.

Fd−FNR complexes showed a broad range of NADPH-dependent cyt *c* reductase activities (black bars in Figure 4). No Fd−FNR complex displayed a significantly higher activity than the dissociable wild-type Fd/FNR (FNR with a saturating amount of Fd). Although the decrease in activity among the various complexes is rather continuous, their activity can be categorized into three major groups according to the linkage sites between Fd and FNR: Fd2C or -4C and FNR1C or -2C with more than 70% activity in comparison to wild-type Fd/FNR (group I), Fd1C or -5C, and FNR1C or -2C with intermediate activity (7−46%) (group II), and Fd3C and any FNR Cys mutants, together with FNR3C and any Fd Cys mutants resulting in less than 3% activity (group III). Thus, the activity tends to be higher when Fd and FNR residues relatively close to each redox center were used for the linkage, as expected (see Figure 1). Activity of the Fd−FNR complexes showed a linear dependence on its concentration as exemplified in Figure 5, which indicates an electron transfer from FNR to Fd domains within the complex rather than between different complexes. The K_m values for cyt *c* among the different groups of Fd−FNR complexes in this reaction were shown to be similar (14−18 μM), and NADPH-dependent diaphorase activity of the Fd−FNR complexes with 2,6-dichlorophenolindophenol (DCPIP) as electron acceptor has been shown previously not to be largely different from that of wild-type FNR under the current experimental conditions (*18*). These results indicate that the differences in the cyt *c* reductase activity among the various Fd−FNR complexes are mostly due to different intramolecular electron transfer activity from FNR to Fd domains.

Addition of wild-type Fd to the assay mixtures increased the activity with all Fd−FNR combinations tested although to a different extent, as exemplified in Figure 6: Slight and significant increases were seen with group I and II complexes, respectively, while the almost negligible activity of group III complexes was considerably recovered. Therefore, even if the intramolecular electron transfer from FNR to Fd moieties of group III complexes is inefficient, the redox centers (FAD) of their FNR moiety appear to be accessible for free Fd, similar to or even better than those of group I and II.

Ionic Strength Dependence of Cyt c Reductase Activity. As the Fd:FNR complex is known to be stabilized by electrostatic interactions involving specific charged side chains, the effect of Fd−FNR linkage on the ionic strength dependence of the cyt *c* reductase activity was investigated using two different group I complexes (Figure 7). Their profiles were similar to that of dissociable wild-type Fd/FNR, influenced by ionic strength in a complex biphasic fashion, which has been explained by the

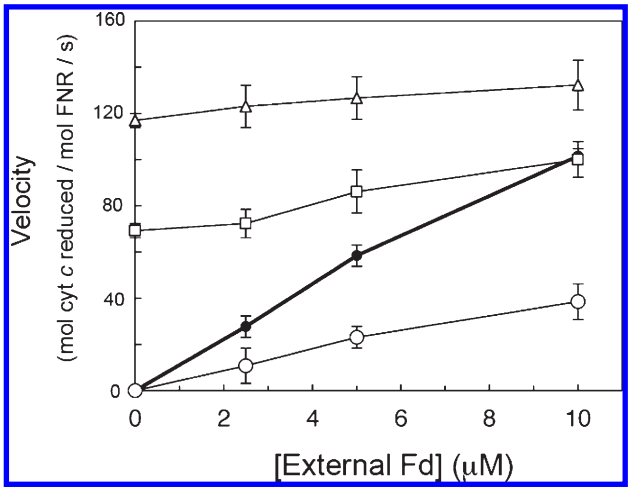

FIGURE 6: NADPH-dependent cyt *c* reductase activities of Fd−FNR cross-linked complexes and wild-type FNR (at 20 nM) in the presence of different concentrations of wild-type Fd. Activities of representative complexes from each group described in the text are shown: wild-type FNR (closed circle), Fd2C−FNR1C (group I, open triangle), Fd1C−FNR1C (group II, open square), and Fd4C−FNR3C (group III, open circle). The profiles were similar among the same group of the complexes.

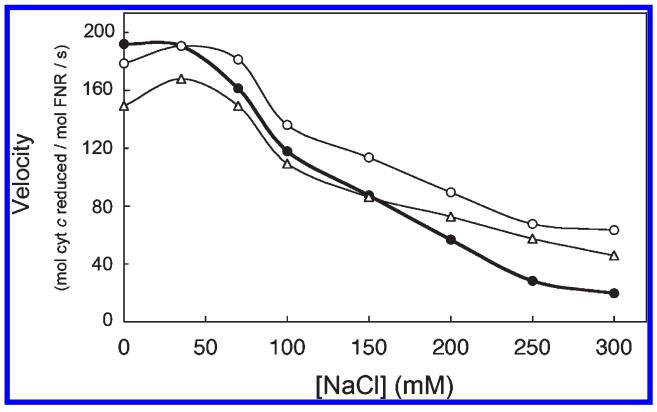

FIGURE 7: Ionic strength dependence of NADPH-dependent cyt *c* reductase activities of dissociable wild-type Fd/FNR (closed circle, 20 nM FNR and 20 μM Fd) and two group I complexes (20 nM), Fd2C−FNR1C (open triangle) and Fd4C−FNR1C (open circle). The reactions were performed in the presence of different concentrations of NaCl (at 0−300 mM).

different contribution of electrostatic and hydrophobic interactions depending on the ionic strength (*11*). However, the activity of the cross-linked complexes generally remained higher with increasing ionic strength: At 300 mM NaCl, their activity was about 2−3 times higher than that of Fd/FNR, with Fd2C−FNR1C and Fd4C−FNR1C showing 27% and 33% of their maximum activity, respectively, in comparison to only 10% in the case of Fd/FNR. In conclusion, disulfide linkage between Fd and FNR resulted in higher stability against the disruption of the electrostatic interaction in the complex by NaCl.

Stopped-Flow Analysis. In order to estimate the rate of electron transfer from FNR to Fd in cross-linked complexes, reactions between NADPH and Fd−FNR complexes (at 10 μM each) were analyzed by stopped-flow methods using either a photodiode array detector or a single-wavelength detector. Electron transfer from wild-type FNR to Fd, as well as that from Fd to FNR, is too fast to be followed by stopped-flow (rapid mixing) techniques as revealed by *Anabaena* and spinach proteins (*3*, *27*, *28*). However, laser flash photolysis could determine a rate constant (k_{obs}) of about 6000 s^{-1} for the electron transfer from *Anabaena* Fd to FNR (*29*). The rate of NADPH-driven electron transfer from FNR to Fd is not reported, while the rates of FNR reduction by NADPH which takes place via a two-step mechanism have been estimated to be >600 and 100−200 s^{-1} for the first and second steps, respectively, by the stopped-flow technique (*3*).

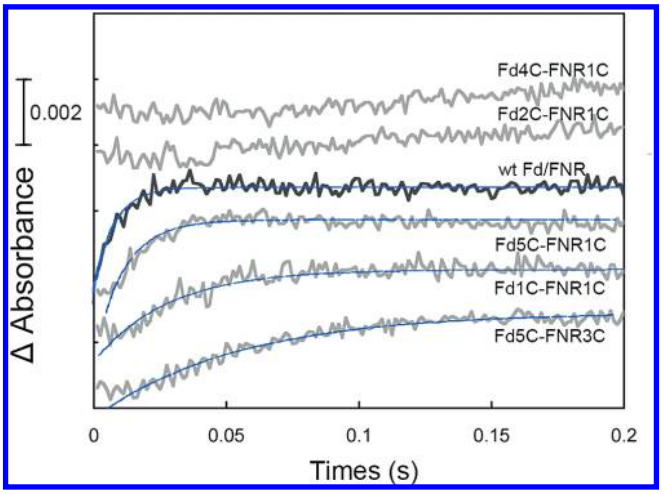

FIGURE 8: Time course of the reactions of NADPH with different Fd−FNR cross-linked complexes or wild-type Fd/FNR (10 μM each) followed at 650 nm. Reactions were carried out as described in Experimental Procedures. Fitting to a monoexponential process (from several ms to 200 ms after mixing) of the lower four traces is shown in dark blue line. The lag phases observed in the lower three traces (group II and III cross-linked complexes) are thought to be either due to an inefficient electron transfer to Fd or due to slow reduction of FNR as well as an inefficient electron transfer to Fd.

Five different Fd−FNR complexes, Fd2C−FNR1C and Fd4C−FNR1C from group I, Fd1C−FNR1C and Fd5C−FNR1C from group II, and Fd5C−FNR3C from group III were used for the analysis. A decrease in a wavelength absorbance around 400−500 nm, which is attributed to FNR reduction by NADPH and subsequent Fd reduction (together with FNR reoxidation), occurred mostly within 0.1 s with the cross-linked complexes and wild-type Fd/FNR (exemplified in Figure 1 of Supporting Information). Absorption changes at 458 nm (absorbance maximum of Fd−FNR complexes) shown in the inset of the figure indicated somewhat slower kinetics of Fd5C−FNR3C (group III) reaction. In addition, a smaller increase in the absorbance at longer than 500 nm occurred within a similar time scale as above, which is thought to be attributed to the production of a semiquinone form of FNR (FNR_{sq}). After the reduction of FNR by NADPH, the reduced form of FNR (FNR_{red}) is converted to FNR_{sq} concomitantly with the reduction of Fd as follows:

$$FNR_{red} + Fd_{ox} \rightarrow FNR_{sq} + Fd_{red}$$

FNR_{sq} exhibits a broad long-wavelength absorption band with a maximum around 600 nm where the protein-bound neutral FAD semiquinone absorbs (*27*). Because virtually no absorbance by FNR_{red} and FNR_{ox} and only small absorbance by Fd_{red} and Fd_{ox} are observed at wavelengths longer than 650 nm, the increase at 650 nm should be mainly ascribed to the formation of FNR_{sq} (extinction coefficients; 2.9 mM^{-1} cm^{-1}) (*27*). On the other hand, the analysis of Fd reduction using isosbestic points for different FNR forms was not simple with this system. Therefore, electron transfer reactions from FNR to Fd were followed at 650 nm. The profile of single-wavelength analysis at 650 nm

varied among the five Fd−FNR complexes tested (Figure 8). For the reactions except those with group I complexes (upper two traces), the observed increases in the absorbance at 650 nm fit a single exponential equation within the time scale from several milliseconds to 200 ms after mixing, with observed rate constants (k_{obs}) of 102 ± 12, 81.8 ± 10.3, 54.0 ± 8.8, and 17.9 ± 1.4 s^{-1} (n = 3−5) for 10 μM each of wild-type Fd/FNR, Fd5C−FNR1C, Fd1C−FNR1C and Fd5C−FNR3C, respectively. On the other hand, relatively flat but slightly concave curves were observed with the two group I complexes. The exact reason for this is not clear at present. A simple explanation for this may be that they display much faster electron transfer from FNR_{red} to Fd_{ox} occurring within the dead time of our instrument (~2 ms). Alternatively, a different kinetic mechanism may operate with these artificially cross-linked complexes. Absorbance around 650 nm has been also observed with charge transfer complexes formed during the reduction of FNR by NADPH (*28*). However, analysis of the reaction between 10 μM each of NADPH and FNR at 458 nm indicated that FNR reduction occurred within 20 ms ($k_{obs} = 111 \pm 6$ s^{-1} or more), consistent with the previous report described above, and the final traces at 650 nm in the same reaction were hardly detectable probably due to the smaller extinction coefficient of the charge transfer complexes (about 1 mM^{-1} cm^{-1}) (*28*). Thus, if the electron transfer rate from FNR_{red} to Fd_{ox} is comparable to or faster than the rate of FNR reduction, changes in the absorbance at 650 nm may not be observed, because FNR_{sq} is expected to form promptly after (almost simultaneously with) the conversion of the charge transfer complex to FNR_{red}. Increasing the concentration of Fd in the reaction of wild-type Fd/FNR up to a saturating amount (40 μM) appeared to increase the k_{obs} values, but the detection of the phase which exhibits exponential increase of the absorbance became more difficult ($k_{obs} > 140$ s^{-1}). This is consistent with the previous report (*29*) that electron transfer from wild-type Fd to FNR becomes rate-limiting only at higher FNR concentrations, whereas at lower concentrations, complex formation limits the rate under 100 mM of ionic strength. Thus, the results of stopped-flow analysis are compatible with those of cyt *c* reduction activity at least with group II and III complexes although the k_{obs} for the group III complex appears to be higher than that estimated from the rate of cyt *c* reduction (k_{cat} of 2−3 s^{-1}).

NMR Chemical Shift Perturbation Analysis. In order to investigate the structure of these cross-linked complexes, we analyzed the FNR interaction sites on the Fd domain by an NMR chemical shift perturbation. Two complexes from each of group I (Fd2C−FNR1C and Fd4C−FNR1C) and group III (Fd2C−FNR3C and Fd4C−FNR3C) were selected for the analysis. ^{1}H and ^{15}N heteronuclear single-quantum correlation (HSQC) spectra of ^{15}N-labeled wild-type Fd, Fd2C, and Fd4C have been determined. As observed in previous analyses of the same wild-type Fd (*5*, *24*), the amide resonances of most Fd residues were readily detected except for those close to the [2Fe-2S] cluster due to paramagnetic relaxation enhancement by the iron (Figure 2A of Supporting Information). The HSQC spectra of Fd2C and Fd4C were very similar to wild-type Fd except for the amide resonances at positions 21 and 22, and at position 59, which could not be assigned in Fd2C and Fd4C, respectively. HSQC spectra of the four Fd−FNR complexes containing ^{15}N-labeled Fd (Fd2C or Fd4C) were measured. As a control, HSQC spectra of the same samples were also measured in the presence of DTT which cleaves the disulfide bond between Fd and FNR domains of the cross-linked complexes, resulting in dissociable mutant Fd and FNR (exemplifying Fd2C-containing Fd−FNR complexes in Figure 2D of Supporting Information). Chemical shift perturbations of Fd in the four Fd−FNR complexes, in the presence and absence of DTT, are shown in Figure 9A. Blue bars show changes in the chemical shifts of the Fd−FNR complexes from those of corresponding free Fd, and red bars show the chemical shift changes after addition of DTT. The pattern after addition of DTT (red bars) is quite similar among the four Fd−FNR complexes and also similar to that of wild-type Fd/FNR (Figure 2B of Supporting Information), as expected because they all represent the interaction mode of separate, dissociable Fd/FNR. In contrast, the pattern in the absence of DTT (blue bars) is different among the four Fd−FNR complexes although rather similar within the two group I complexes (upper panels). Moreover, the patterns between the presence (red bars) and absence (blue bars) of DTT within each Fd−FNR complex are more similar in the two group I complexes than in the other two group III complexes. This indicates that FNR interaction sites on the Fd domain of the group I Fd−FNR complexes are more similar to those of dissociable Fd/FNR, as compared to those of the group III complexes. Three-dimensional mapping of these chemical shift changes on the Fd molecule (Figure 9B) visualized the similarity of the FNR binding region between Fd/FNR and the two group I complexes (upper panels) and the large difference between Fd/FNR and the two group III complexes (lower panels). Besides such an observation, it is noteworthy that there is a smaller but significant difference in the patterns between the two Fd−FNR complexes in group I (see blue bars of the two upper panels of Figure 9A), although they can attain a similar level of electron transfer activity comparable to that of Fd/FNR.

Absorption Spectral Analysis. In order to investigate the environment around the prosthetic groups of the four Fd−FNR complexes, we measured their absorption spectra. Absorption around 380 and 460 nm, derived from the flavin component of FNR, is known to increase by complex formation with Fd, which indicates the changes in the environment around the redox center of FNR. Figure 10 shows the absorption spectra of wild-type Fd/FNR and the four Fd−FNR complexes under low ionic strength condition (black lines) in comparison with control spectra which have been recorded in the presence of DTT only (red lines) or DTT plus 0.5 M NaCl (blue lines). The spectra obtained in the presence of DTT only (red lines) are basically the same for all complexes, representing absorption of the dissociable Fd:FNR complex after cleavage of linkage between Fd and FNR. Similarly, the spectra obtained in the presence of DTT and NaCl (blue lines) are also basically the same for all complexes, representing the decreased absorption of unbound Fd and FNR after disruption of electrostatic interaction between the two proteins. Spectra of the two group I Fd−FNR complexes (black lines in upper right, two panels) are more similar to those in the presence of DTT (red lines) while the spectra of the other two group III complexes (black lines in lower panels) are more similar to those in the presence of DTT and NaCl (blue lines). These results indicate that the environment of FAD in group I Fd−FNR complexes is more similar to that of the native Fd:FNR complex while the environment of group III is more similar to that of the free (unbound) state of Fd and FNR. A similar phenomenon was observed with spectral analysis (Figure 3) of another group III complex, Fd5C−FNR3C, which showed a spectrum close to that of unbound (computed) Fd and FNR. Difference spectra among the three spectra of each Fd−FNR

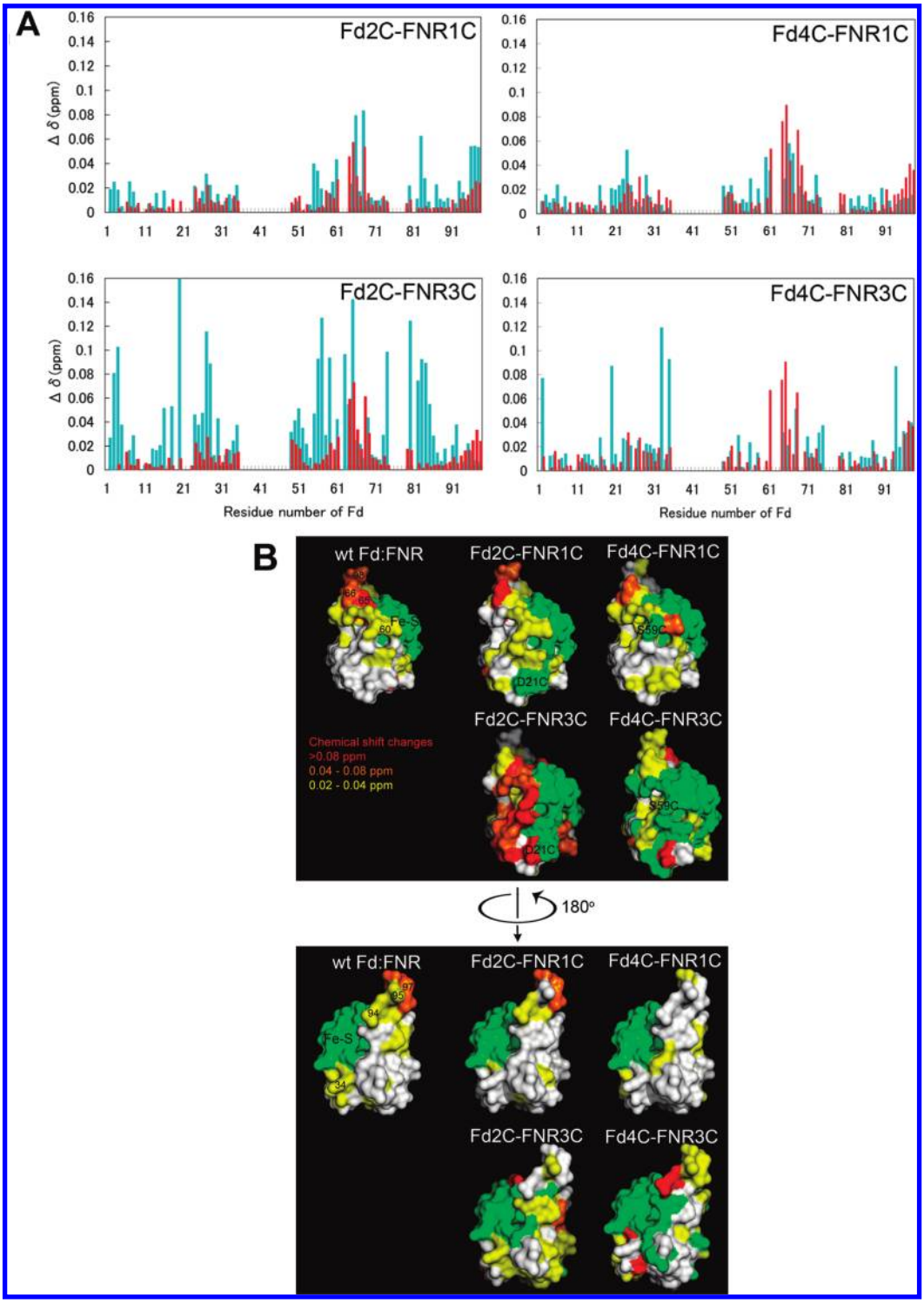

FIGURE 9: (A) Weighted averages of the ^{1}H and ^{15}N chemical shift changes on the HSQC spectra of four Fd−FNR cross-linked complexes, with two from group I (upper panels) and two from group III (lower panels), in the presence (red bars) and absence (blue bars) of DTT, from those of the corresponding free Fd, plotted against the Fd residue number. (B) Mapping of the chemical shift changes on the three-dimensional structure of Fd (Protein Data Bank entry 1GAQ) viewed from two different sides. Residues are colored according to color codes: 0.02−0.04 ppm (yellow), 0.04−0.08 ppm (orange), and >0.08 ppm (red). Residues near the [2Fe-2S] cluster, whose chemical shift data are not available due to the paramagnetic effect of the iron, are shown in green. The chemical shift changes of "wt Fd:FNR" were obtained from the titration of labeled Fd with FNR as presented in Figure 2A−C of Supporting Information. The figure was produced with PyMol (*40*). The sites for Cys substitutions on the Fd molecule are indicated as "D21C" and "S59C".

complex in Figure 10 provide a more detailed comparison and more significant differences in the shape of the spectra even within the same group, suggesting variations in the FAD environment (Figure 3 of Supporting Information). Therefore, the microenvironment of FAD among the four Fd−FNR complexes can be roughly categorized into two groups, but the precise FAD environment varied from one to another.

These two structural analyses indicate that two Fd−FNR complexes from group I which exhibit higher cyt *c* reduction activity assume a Fd−FNR interaction mode similar to that of

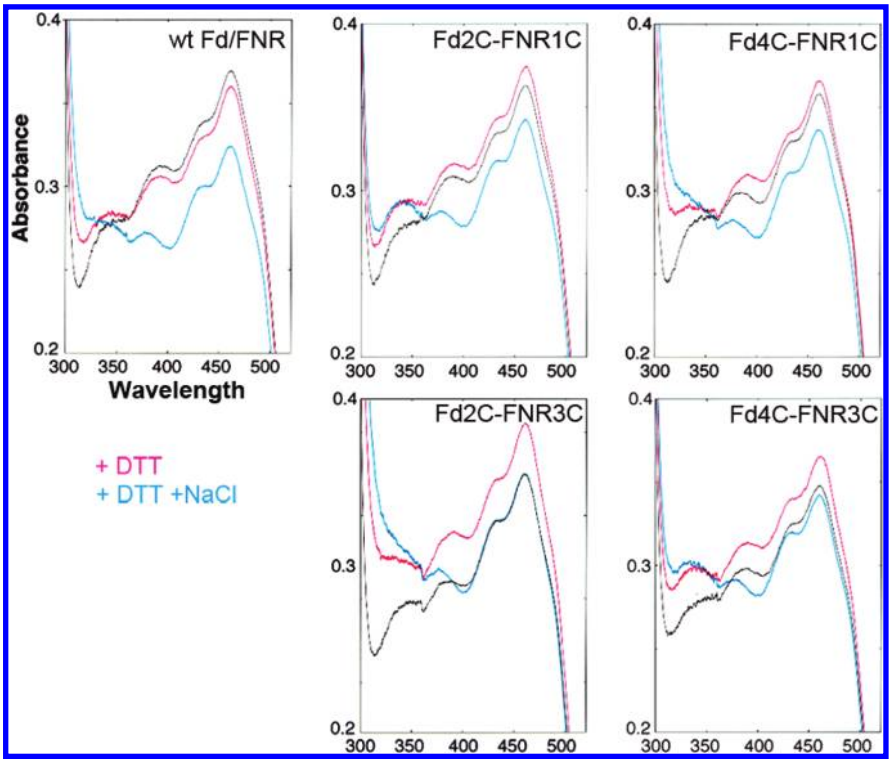

FIGURE 10: Absorption spectra of wild-type Fd/FNR (at 1:1 ratio) and four Fd−FNR cross-linked complexes (at 20 μM), with two from group I (upper panels) and two from group III (lower panels), in the presence (red line) and absence (black line) of DTT (at 4 mM) under low ionic strength condition (in 20 mM Tris-HCl, pH 7.5) and in the presence of DTT and 0.5 M NaCl (blue line).

the native Fd:FNR complex while the interaction mode of the other two group III complexes with the lower activity are very different from that of the native complex.

NADPH-Dependent Nitrite Reductase (*NiR*) *Activity* (*NADPH*/*FNR*/*Fd*/*NiR*). We next examined the function of the various Fd−FNR complexes as a mobile electron carrier. Fd is best known for its role in photosynthetic electron transport, accepting electrons from photosystem I (PS I) and donating them to FNR for photoreduction of $NADP^+$, but it also donates electrons to many other plastid enzymes including those essential for reductive assimilation of sulfur and nitrogen such as sulfite reductase and NiR (*30*). For this reason, the activity of various Fd−FNR complexes with these processes was investigated. Electron transfer from the complexes to NiR with NADPH as electron donor (gray bars in Figure 4) yielded activity levels from those comparable to the dissociable Fd/FNR down to less than 7% of this activity. However, the trend in these activity levels was completely different from that observed for the cyt *c* reductase (gray bars vs black bars in Figure 4), correlating with the FNR-linkage site on the Fd domain with the descending order of Fd5C, 3C > Fd1C > Fd4C > Fd2C (as rearranged in Figure 4 of Supporting Information). These results indicate that electron transfer from the Fd−FNR complexes to NiR depends on the FNR-linkage site on the Fd domain; the closer the linkage site is to the [2Fe-2S] cluster of the Fd domain (see Figure 1), the lower is the electron transfer activity to NiR. This is probably because NiR binds Fd in a region near the [2Fe-2S] cluster.

Photoreduction of $NADP^+$ (*PS I*/*Fd*/*FNR*/$NADP^+$). Electron transfer from PS I, a large Fd-binding protein complex, to the Fd−FNR complexes was determined by the reduction of $NADP^+$ upon illumination of thylakoid membranes that had been prepared from chloroplasts containing endogenous FNR (white bars in Figure 4, and Figure 4 of Supporting Information). Overall, the trend is relatively similar to that observed for NiR. However, the decrease in the photoreduction activity does not seem to be continuous, but rather the activity appears to be divided into two groups depending on the FNR-linkage site on the Fd domain of the complexes: Fd3C, 5C, 1C > Fd4C, 2C. The relative activities of the complexes comprised of Fd2C and Fd4C are considerably lower than for NiR, with the exception of Fd4C−FNR3C (the reason for this is not clear at present).

In this assay, externally added FNR is known to be considerably less efficient in $NADP^+$ photoreduction than endogenous FNR bound to thylakoid membranes (*31*). Therefore, the relatively higher activity of the Fd−FNR complexes, which is comparable to the control reaction in the presence of endogenous FNR and free Fd (at first left column in the figures), indicates that either Fd-linked FNR somehow reconstitutes efficient $NADP^+$ reduction or endogenous FNR bound to membranes, in place of the FNR moiety of the Fd−FNR complexes, catalyzes $NADP^+$ reduction by receiving an electron from the Fd moiety.

DISCUSSION

In this study, cross-link was introduced with a view to physically and systematically change the interaction mode between Fd and FNR, using a short S−S bond linker. The anticipated effect of the cross-linking could be through changes in the distance, orientation, and environment around the redox centers for intramolecular electron transfer and through changes in the affinity (accessibility) of Fd-binding proteins for intermolecular electron transfer. No Fd−FNR complexes with significantly higher cyt *c* reduction activity than the wild-type Fd/FNR (with a saturating amount of Fd) have been obtained in this study, possibly because the molecular interaction between leaf Fd and FNR has been ideally optimized during evolution. Alternatively,

although large excess amount of NADPH and its regeneration system ensure the efficient supply of NADPH in the cyt *c* reduction assay, it is possible that FNR reduction by NADPH, not the electron transfer from FNR to Fd, may be the rate-limiting step especially when group I complexes are used. On the other hand, when compared to the activity of the wild-type Fd/FNR in the presence of equimolar Fd, the cyt *c* reduction activity of group I complexes is much higher (wild-type FNR in the presence of 0.02 μM external Fd vs group I complex in the absence of external Fd in Figure 6). Therefore, in this context, linkage of the two proteins conferred a remarkable increase in electron transfer efficiency. In addition to the location of the linkage sites, the flexibility of the linkage region of the FNR moiety appears to affect the activity; the linkages at positions 19 and 25 of FNR (FNR1C, -2C) with any Fd mutant except Fd3C (at position 53) showed considerable activity, but the linkages at position 36 of FNR (FNR3C) with any Fd mutant caused very low activity (group III) although the distance of these three positions from FAD is similar. This is probably because the N-terminal loop region of FNR (shown as a magenta line in Figure 1), which is expected to be disordered and unrestrained (*32*), can work as a long arm when linked to Fd at this region, allowing a rather proper interaction between the linked Fd and FNR domains. This property appears to be more pronounced when linked via residue 19 of FNR (FNR1C) than via residue 25 (FNR2C) (see the activities of complexes involving FNR1C vs FNR2C in Figure 4) as expected from the difference in the length of the arm formed upon cross-linking. On the other hand, linkage via residue 36 of FNR (FNR3C), which is located at the end of the N-terminal loop region of FNR that appears to be more restrained, probably does not allow such an interaction in any combination with Fd mutants.

In the stopped-flow analysis, the observed rate of electron transfer from FNR to Fd is lowered by a factor of 10^2 to 10^3 in the two group II (54 and 82 s^{-1}) and one group III (18 s^{-1}) complexes, in comparison to the known electron transfer rate of about 6000 s^{-1}, which was obtained by the reaction from Fd_{red} to FNR_{ox} (*29*). The reverse reaction, from FNR_{red} to Fd_{ox}, may be slower than this rate, because it is nonphysiological direction, and redox potential of photosynthetic Fd is lower than that of FNR (*23*). Distances between the redox centers are 8.8 Å for *Anabaena* and 5.9 Å for maize leaf proteins. The electron transfer rate depends exponentially on the distance between the redox sites in a single step electron tunneling reaction (*17*). It also depends on the energy required to reorganize nuclear coordinates upon charge transfer and the driving force for the electron transfer (*33*). However, electron tunneling theory itself provides only an upper limit for the rate of electron transfer. Many electron transfers in oxidoreductases are limited not by electron tunneling but by slower coupled events of chemistry, conformational changes, or motion (*34*). In fact, although the time table for distance dependence of observed electron transfer rates, proposed by Gray et al. using Ru-modified proteins (*35*), was shown to agree well with multiredox-center complexes of photosynthetic reaction centers and cyt *c* oxidase, electron transfer rate and distance of soluble and dissociable Fd/FNR, described above, seem to largely exceed the time table prediction (e.g., distances of 8.8 and 5.9 Å correspond to the rate of $> 10^{10}$ s^{-1} in the table). Therefore, elucidation of the relationship between the intramolecular electron transfer rate of Fd−FNR complexes and their configuration of Fd/FNR including the distance between the redox centers has to wait for the detailed structural analysis of the complexes. Nevertheless, rough estimation might be made; in a typical protein medium, 1.5 Å distance normally corresponds to an ~10-fold decrease in tunneling rate (*33*). Therefore, assuming that the electron transfer rate of *Anabaena* and maize leaf Fd/FNR is similar, 10^2 to 10^3 decrease in the electron transfer rate in the group II and III complexes corresponds to the distance between their redox centers, which is 3−4.5 Å longer than that of the wild-type Fd:FNR complex (5.9 Å). Such estimated distance, in the case of the group III complex, seems to be shorter than expected from the result of NMR analysis of this group, which showed a large deviation of the FNR binding sites on Fd from native Fd:FNR. In this context, relatively higher k_{obs} compared to the cyt *c* reduction rate, obtained for the group III complex in this study, may be due to the electron transfer between different molecules of this complex (intermolecular electron transfer) at the concentration of 10 μM, whereas the concentration-dependent activity of the complex with cyt *c* reduction assay was linear up to 1.4 μM (Figure 5). Lower concentrations of the complex may be required to obtain a better estimate for the intramolecular electron transfer rate from the FNR to Fd domains, but as observed in Figure 8, absorbance changes at 650 nm are small and almost at the lower limit for the analysis even at 10 μM. Other analyses such as cyt *c* reduction coupled to Fd reduction may be appropriate but may require a more complicated system (e.g., sequential mixing).

Spectral analyses showed that two of the group I complexes assume an Fd−FNR interaction mode similar to that of the native Fd:FNR complex. So far, we have not obtained Fd−FNR complexes that exhibit higher cyt *c* reductase activity but appear to assume configurations dramatically different from that in the leaf Fd:FNR complex, maybe because the binding mode of the leaf Fd and FNR has been intensively optimized by specific interactions. However, we cannot rule out the possibility that any of the other group I or group II complexes may assume a configuration similar to that in the root- or *Anabaena*-type complex, in which Fd is rotated by 60° or 96° (in reverse direction), respectively, relative to FNR compared to its orientation in the leaf-type complex. Precise structure analyses of the Fd−FNR complexes should clarify this possibility.

Electron transfer with NiR and PS I was largely inhibited in assays where the Fd−FNR complexes that showed higher cyt *c* reduction activity (such as group I) were used. In contrast, most of the complexes that displayed lower cyt *c* reduction activity (group III) showed considerable electron transfer activity in these assays. This is because the cyt *c* reduction assay is intended to measure the activity of Fd reduction by NADPH via FNR, while NiR and photoreduction assays are intended to evaluate the affinity between Fd−FNR complexes and NiR or PS I. The latter function appears to be poor in group I complexes compared to group II and III complexes. Such intermolecular electron transfer activity appears to depend basically on the FNR-linkage site on the Fd domain. Previous studies such as those using mutagenesis (*36*, *37*) and our recent NMR analysis (unpublished; manuscript in preparation) revealed the probable NiR binding region on Fd, which overlaps but partly differs from that of FNR. Therefore, binding of NiR to the Fd moiety becomes more difficult if the FNR-linkage site approaches the putative NiR binding sites around the cluster. Although less information is available, in the case of PS I, involvements of the C-terminal region of Fd (*38*) and a certain acidic area in the vicinity of the [2Fe-2S] cluster (*39*) have been suggested.

Overall, this study showed that linkage of Fd and FNR by different single disulfide bonds resulted in a series of Fd−FNR

complexes which exhibit reciprocal activities of intramolecular and intermolecular electron transfer. This could explain why Fd and FNR in chloroplasts are present as separate proteins instead of being constantly linked together as observed in some bacterial flavoreductase; i.e., Fd must be a mobile protein in chloroplasts.

Combinations of three-dimensional structure analysis and more detailed time-resolved electron transfer analysis of the Fd−FNR complexes should reveal the quantitative and qualitative relationship between the distance (and angle) of the redox centers and the electron transfer rate of Fd and FNR in detail. The series of synthetic Fd−FNR complexes produced in this study could be a suitable tool for the investigation of such a relationship, which would be difficult to achieve with collections of various natural proteins.

SUPPORTING INFORMATION AVAILABLE

Time course of spectral changes accompanying the reaction of 10 μM NADPH with 10 μM Fd−FNR cross-linked complex (Fd2C−FNR1C) (Figure S1), NMR chemical shift perturbation analysis of wild-type (wt) Fd upon complex formation with wt FNR and of Fd2C mutant upon cross-linking with FNR1C or FNR3C mutant (Figure S2), difference spectra among three absorption spectra from each of wild-type Fd/FNR and four Fd−FNR complexes shown in Figure 10 (Figure S3), and activities of nitrite reduction and photoreduction of $NADP^+$ with dissociable wild-type Fd/FNR and Fd−FNR complexes in the descending order of nitrite reduction activity (rearrangement of Figure 4) (Figure S4). This material is available free of charge via the Internet at http://pubs.acs.org.

REFERENCES

1. Hanke, G. T., Kurisu, G., Kusunoki, M., and Hase, T. (2004) Fd: FNR electron transfer complexes: evolutionary refinement of structural interactions. *Photosynth. Res. 81*, 317–327.
2. Correll, C. C., Ludwig, M. L., Bruns, C. M., and Karplus, P. A. (1993) Structural prototypes for an extended family of flavoprotein reductases: comparison of phthalate dioxygenase reductase with ferredoxin reductase and ferredoxin. *Protein Sci. 2*, 2112–2133.
3. Carrillo, N., and Ceccarelli, E. A. (2003) Open questions in ferredoxin-$NADP^+$ reductase catalytic mechanism. *Eur. J. Biochem. 270*, 1900–1915.
4. Karlsson, A., Beharry, Z. M., Eby, D. M., Coulter, E. D., Neidle, E. L., Burtz, D. M., Jr, Eliund, H., and Ramaswamy, S. (2002) X-ray crystal structure of benzoate 1,2-dioxygenase reductase from *Acinetobacter* sp. strain ADP1. *J. Mol. Biol. 318*, 261–272.
5. Kurisu, G., Kusunoki, M., Katoh, E., Yamazaki, T., Teshima, K., Onda, Y., Kimata-Ariga, Y., and Hase, T. (2001) Structure of the electron transfer complex between ferredoxin and ferredoxin-$NADP^+$ reductase. *Nat. Struct. Biol. 8*, 117–121.
6. Morales, R., Kachalova, G., Vellieux, F., Charon, M.-H., and Frey, M. (2000) Crystallographic studies of the interaction between the ferredoxin-$NADP^+$ reductase and ferredoxin from the cyanobacterium, *Anabaena*: looking for the elusive ferredoxin molecule. *Acta. Crystallogr. D 56*, 1408–1412.
7. Pettigrew, G. W., and Seilman, S. (1982) Purification and properties of a cross-linked complex between cytochrome *c* and cytochrome *c* peroxidase. *Biochem. J. 201*, 9–18.
8. Guo, M., Bhasker, B., Li, H., Barrows, T. P., and Poulos, T. L. (2004) Crystal structure and characterization of a cytochrome *c* peroxidase-cytochrome *c* site-specific cross-link. *Proc. Natl. Acad. Sci. U.S.A. 101*, 5940–5945.
9. Zanetti, G., Aliverti, A., and Curti, B. (1984) A cross-linked complex between ferredoxin and ferredoxin-$NADP^+$ reductase. *J. Biol. Chem. 259*, 6153–6157.
10. Colvert, K. K., and Davis, D. J. (1988) Characterization of a covalently linked complex involving ferredoxin and ferredoxin: NADP reductase. *Photosynth. Res. 17*, 231–245.
11. Aliverti, A., and Zanetti, G. (1997) A three-domain iron-sulfur flavoprotein obtained through gene fusion of ferredoxin and ferredoxin-$NADP^+$ reductase from spinach leaves. *Biochemistry 36*, 14771–14777.
12. Lacour, T., and Ohkawa, H. (1999) Engineering and biochemical characterization of the rat microsomal cytochrome P4501A1 fused to ferredoxin and ferredoxin-$NADP^+$ reductase from plant chloroplasts. *Biochim. Biophys. Acta 1433*, 87–102.
13. Munro, A. W., Girvan, H. M., and McLean, K. J. (2007) Cytochrome P450-redox partner fusion enzymes. *Biochim. Biophys. Acta 1770*, 345–359.
14. Gassner, G. T., and Ballou, D. P. (1995) Preparation and characterization of a truncated form of phthalate dioxygenase reductase that lacks an iron-sulfur domain. *Biochemistry 34*, 13460–13471.
15. Blazyk, J. L., and Lippard, S. J. (2002) Expression and characterization of ferredoxin and flavin adenine dinucleotide binding domain of the reductase component of soluble methane monooxygenase from *Methylococcus capsulatus* (Bath). *Biochemistry 41*, 15780–15794.
16. Neeli, R., Girvan, H. M., Laurence, A., Warren, M. J., Leys, D., Scrutton, N. S., and Munro, A. W. (2005) The dimeric form of flavocytochrome P450 BM3 is catalytically functional as a fatty acid hyrdoxylase. *FEBS Lett. 579*, 5582–5588.
17. Marcus, R. A., and Sutin, N. (1985) Electron transfers in chemistry and biology. *Biochim. Biophys. Acta 881*, 265–322.
18. Kimata-Ariga, Y., Sakakibara, Y., Ikegami, T., and Hase, T. (2008) NMR analysis of ferredoxin tethered to ferredoxin-$NADP^+$ reductase in various configurations, in Proceedings of the Sixteenth International Symposium on Flavins and Flavoproteins (Frago, S., Gomez-Moreno, C., and Medina, M., Eds.) pp 99−106, Prensas Universitarias de Zaragoza, Zaragoza.
19. Matsumura, T., Kimata-Ariga, Y., Sakakibara, H., Sugiyama, T., Murata, H., Takao, T., Shimonishi, Y., and Hase, T. (1999) Complementary DNA cloning and characterization of ferredoxin localized in bundle-sheath cells of maize leaves. *Plant Physiol. 119*, 481–488.
20. Onda, Y., Matsumura, T., Kimata-Ariga, Y., Sakakibara, H., Sugiyama, T., and Hase, T. (2000) Differential interaction of maize root ferredoxin: $NADP^+$ oxidoreductase with photosynthetic and non-photosynthetic ferredoxin isoproteins. *Plant Physiol. 123*, 1037–1045.
21. Sekine, K., Sakakibara, Y., Hase, T., and Sato, N. (2009) A novel variant of ferredoxin-dependent sulfite reductase having preferred substrate specificity for nitrite in the unicellular red alga *Cyanidioschyzon maerolae*. *Biochem. J. 423*, 91–98.
22. Marzinzig, M., Nussler, A. K., Stadler, J., Marzinzig, E., Barthlen, W., Nussler, N. C., Berger, H. g., Morris, S. M., Jr., and Bruckner, U. B. (1997) Improved methods to measure end products of nitric oxide in biological fluids: nitrite, nitrate, and *S*-nitrosothiols. *Nitric Oxide 1*, 177–189.
23. Hanke, G. T., Kimata-Ariga, Y., Taniguchi, I., and Hase, T. (2004) A post genomic characterization of *Arabidopsis* ferredoxins. *Plant Physiol. 134*, 255–264.
24. Saitoh, T., Ikegami, T., Nakayama, M., Teshima, K., Akutsu, H., and Hase, T. (2006) NMR study of the electron transfer complex of plant ferredoxin and sulfite reductase. *J. Biol. Chem. 281*, 10482–10488.
25. Kimata-Ariga, Y., Saitoh, T., Ikegami, T., Horii, T., and Hase, T. (2007) Molecular interaction of ferredoxin and ferredoxin-$NADP^+$ reductase from human malaria parasite. *J. Biochem. 142*, 715–720.
26. Delaglio, F., Grzesiek, S., Vuister, G. W., Zhu, G., Pfeifer, J., and Bax, A. (1995) NMRPipe: a multidimensional spectral processing system based on UNIX pipes. *J. Biomol. NMR 6*, 277–293.
27. Batie, C. J., and Kamin, H. (1984) Electron transfer by ferredoxin: $NADP^+$ reductase. *J. Biol. Chem. 259*, 11976–11985.
28. Tejaro, J., Peregrina, J. R., Martinez-Julvez, M, Gutierrez, A., Gomez-Moreno, C., Scrutton, N. S., and Medina, M. (2007) Catalytic mechanism of hydride transfer between $NADP^+$/H and ferredoxin-$NADP^+$ reductase from *Anabaena* PCC 7119. *Arch. Biochem. Biophys. 459*, 79–90.
29. Hurley, J. K., Fillat, M. F., Gomez-Moreno, C., and Tollin, G. (1996) Electrostatic and hydrophobic interactions during complex formation and electron transfer in ferredoxin/ferredoxin-$NADP^+$ reductase system from *Anabaena*. *J. Am. Chem. Soc. 118*, 5526–5531.
30. Knaff, D. B., and Hirasawa, M. (1991) Ferredoxin-dependent chloroplast enzymes. *Biochim. Biophys. Acta 1056*, 93–125.
31. Forti, G., Cappelletti, A., Nobili, R. L., Garlaschi, F. M., Gerola, P. D., and Jennings, R. C. (1983) Interaction of ferredoxin and ferredoxin-NADP reductase with thylakoids. *Arch. Biochem. Biophys. 221*, 507–513.
32. Karplus, P. A., Daniels, M. J., and Herriot, J. R. (1991) Atomic structure of ferredoxin-$NADP^+$ reductase: prototype for a structurally novel flavoenzyme family. *Science 251*, 60–66.
33. Page, C. C., Moser, C. C., Chen, X., and Dutton, P. L. (1999) Natural engineering principles of electron tunnelling in biological oxidation-reduction. *Nature 402*, 47–52.
34. Moser, C. C., Page, C. C., and Dutton, P. L. (2006) Darwin at the molecular scale: selection and variance in electron tunnelling proteins

including cytochrome *c* oxidase. *Philos. Trans. R. Soc. London, Ser. B 361*, 1295–1305.
35. Gray, H. B., and Winkler, J. R. (2003) Electron tunneling through proteins. *Q. Rev. Biophys. 36*, 341–372.
36. Garcia-Sanchez, M. I., Gotor, C., Jacquot, J. P., Stein, M., Suzuki, A., and Vega, J. M. (1997) Critical residues of *Chlamydomonas reinhardtii* ferredoxin for interaction with nitrite reductase and glutamate synthase revealed by site-directed mutagenesis. *Eur. J. Biochem. 250*, 364–368.
37. Garcia-Sanchez, M. I., Diaz-Quintana, A., Gotor, C., Jacquot, J. P., De la Roma, M. A., and Vega, J. M. (2000) Homology predicted structure and functional interaction of ferredoxin from the eukaryotic alga *Chlamydomonas reinhardtii* with nitrite reductase and glutamate synthase. *J. Biol. Inorg. Chem. 6*, 713–719.
38. Lelong, C., Setif, P., Lagoutte, B., and Bottin, H. (1994) Identification of the amino acid involved in the functional interaction between photosysytem I and ferredoxin from *Synechocystis* sp. PCC 6803 by chemical cross-linking. *J. Biol. Chem. 269*, 10034–10039.
39. Guillouard, I., Lagoutte, B., Noal, G., and Bottin, H. (2000) Importance of the region including aspartates 57 and 60 of ferredoxin on the electron transfer complex with photosystem I in the cyanobacterium *Synechocystis* sp. PCC 6803. *Biochem. Biophys. Res. Commun. 271*, 647–653.
40. DeLano, W. L. (2002) The PyMol Molecular Graphics system, DeLano Scientific, San Carlos, CA (http://www.pymol.org).